Asian Journal of Chemistry; Vol. 36, No. 12 (2024), 2783-2789

ASIAN JOURNAL OF CHEMISTRY

https://doi.org/10.14233/ajchem.2024.32676

A Simple Hydrothermally Prepared CuO Nanoparticles for Enhanced Supercapacitor Applications

M. SEETHALAKSHMI[1], M. SHANTHI[2,*], S. DHANAPANDIAN[1] and K. ASHOKKUMAR[3]

[1]Department of Physics, Annamalai University, Annamalainagar-608002, India
[2]Department of Physics, Government Arts College for Women, Sivagangai-630562, India
[3]Department of Physics, V.R.S. College of Engineering & Technology, Arasur, Villupuram-607107, India

*Corresponding author: E-mail: shanthi9962562962@gmail.com

Received: 8 September 2024; *Accepted*: 16 October 2024; *Published online*: 30 November 2024; AJC-21818

In this study, copper oxide nanoparticles (CuO NPs) were synthesized through a simple hydrothermal route with various surfactants (PEG, CTAB and HMTA) and studied for their phase structure, chemical bonding, surface morphology, oxidation states and electrochemical behaviour. The X-ray diffraction peaks were revealed the orthorhombic structure of the PEG assisted CuO nanoparticles with calculated crystallite size value of 13.23 nm. The SEM images exposed with different morphology such as spherical, rock-like, rod and plate of synthesized products, whereas the XPS analysis revealed the composition and elemental state of the prepared sample. In the FTIR, the presence of vibrational groups in the synthesized material are confirmed. The prepared electrode revealed pseudocapacitance nature and its C_{sp} value of 297 F g^{-1} at 10 mV/s. The stability result indicates that the maximum retention value of 77.24% in the prepared electrode. Moreover, the EIS measurements revealed the exceptional rate capability and reversible characteristics.

Keywords: Hydrothermal, Electrochemical, Morphology, Supercapacitors, Cyclic voltammetry.

INTRODUCTION

The need for clean, safe and sustainable energy is one of the most important issues of the 21st century, as worldwide energy demand continues to increase [1,2]. Over the last few years, huge efforts have been made by several researchers to improve the performance of supercapacitor electrode materials to increase energy capacity and also high power efficiency. Among the different renewable energy storage technologies, super-capacitors have made significant impact in energy systems [3-5]. Basically, the supercapacitors are classified by two types of charge storage mechanisms: (i) electrical double-layer capacitors (EDLC) and (ii) capacitive or pseudocapacitive, which determine the electrochemical performance of product [6-8]. The charge-discharge mechanisms of the pseudocapacitors are based on electron transfer between the electrode, electrolyte interaction and EDLC showed by electrostatic adsorption of electrolyte ions onto the surface of carbon nature with high porosity materials [9-12]. Thus, the researchers have focused on superior pseudo-capacitive behaviour of transition metal oxide with high specific capacitance nature [13,14]. Therefore, many studies have been devoted to exploring low-cost metal oxides, which are considered potential candidates for super-capacitor electrodes such as NiO, MnO_2, SnO_2, CuO, TiO_2 and V_2O_5 [15-19].

Recently, CuO has been studied as an suitable material for pseudocapacitor electrodes due to its cost effective, copious resources, sustainable, fast cycle stability and easy synthesis [20]. Recently, significant efforts have been focused on different types of CuO nanostructured material with various surface morphologies, such as, flower, rock, spherical, rod, nanotubes and hollow spheres. Added surfactants, which tune the surface morphology, enhance surface area and also improve electrochemical behaviour [21]. The CuO electrode nanomaterials are prepared by different methods, such as including sol-gel synthesis [22], co-precipitation [23] and hydrothermal method [24]. Among these methods, the hydrothermal technique stands out as the most effective for synthesizing CuO nanoparticles, owing to its high efficiency, low processing temperature and capability to regulate crystallite size, morphologies, stability and processing versatility [25]. The synthesis of phase-CuO nanoparticles at low temperatures with controlled size and morpho-

logy is the major advantage of the hydrothermal method. In this work, various surfactants(PEG, CTAB and HMTA) added with CuO nanoparticles were prepared through the high pressure hydrothermal method. The crystallite size, functional group, morphologies were carried out XRD, FTIR and SEM. Furthermore, the prepared CuO products have shown excellent electrochemical properties.

EXPERIMENTAL

Analytical grade copper nitrate (99.9%), NaOH (99.9%), polyethylene glycol (PEG, 99.9%), cetyltrimethylammonium bromide (CTAB, 99.9%) and hexamethylenetetramine (HMTA, 99.9%) were procured from commercial suppliers and used as received.

Synthesis of CuO nanoparticles using different surfactants: In this study, CuO nanocrystals were synthesized using a simple hydrothermal approach. A 0.1 M solution of $Cu(NO_3)_2 \cdot 5H_2O$ was prepared by dissolving in 40 mL of deionized water in two separate beakers, followed by stirring for 20 min to achieve homogeneity. Subsequently, 0.05 M of PEG surfactant was mixed into solution B using 30 mL of deionized water and agitated the mixture for 15 min, followed by the addition of solution B into solution A. A precipitating agent consisting of a 0.4M NaOH solution was gradually added dropwise to the aforementioned solution. The synthesized solution was allowed to stir magnetically for another 45 min at room temperature to achieve a homogenous state. Finally, the solution was transferred into a 150 mL autoclave, sealed and maintained in a hot air oven at 170 ºC for 6 h. The resultant digested material underwent filtration to isolate clean products and was subsequently washed with ethanol to eliminate moisture content. Additionally, the filtered precipitate products underwent a drying process in an oven for a duration of 6 h at 100 ºC. Similar methodology was employed utilizing different surfactants *e.g.* CTAB and HMTA.

Characterization: The crystalline phases of the prepared CuO nanomaterials consisted of different surfactants were identified by X-ray diffraction (Shimadzu 6000), whereas the surface morphology was examined using SEM (JSM-6360LA). The chemical condition of the produced electrode material was analyzed using X-ray photoelectron spectroscopy (Thermo-Fisher). The chemical bonding of the sample was identified in the range of 4000 and 400 cm^{-1} using FTIR (Perkin-Elmer Spectrum 2). The multipoint N_2 adsorption and desorption isotherm curves were evaluated using BET (Micromeritics-ASAP). The PEG-CuO nanomaterial was evaluated at several independent scan rates for supercapacitor performance using an electrochemical analyzer (CHI 660).

RESULTS AND DISCUSSION

Powder XRD studies: The XRD peaks of all samples confirmed the presence of diffraction features with various surfactants (CTAB, PEG and HMTA). From Fig. 1, the characteristic peaks at 2θ = 35º, 36º, 38º, 42º, 43º, 58º, 61º, 65º, 68º and 72º, which revealed the orthorhombic crystalline phase, are well matched with JCPDS card No. 77-1898. The peaks present in the spectra correspond to the synthesized CuO nanoparticles as no any additional peaks is revealed [26]. The broad

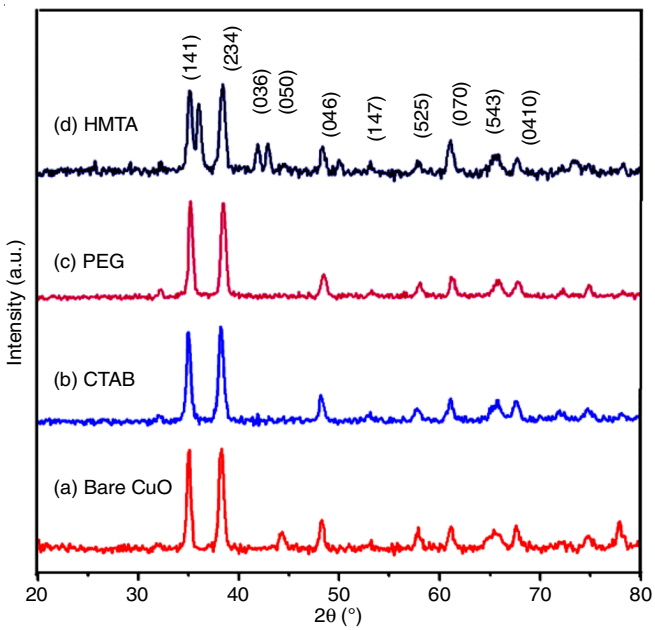

Fig. 1. XRD spectra of CuO with different surfactants

diffraction peaks are obtained from the XRD pattern due to the small crystallite size. The calculated average crystallite size exhibited a slight variation, ranging from 16.19 to 13.23 nm, in reactions employing the different surfactants. The reduced crystallite size of the PEG-assisted CuO nanoparticles typically indicates a greater surface area, leading to an increase in the number of active sites, which contributes to an enhance-ment in specific capacitance characteristics [27].

The various parameters for average crystallite size were calculated by Debye-Scherrer's equation [28]:

$$D = \frac{k \times \lambda}{\beta \cos\theta} \quad (1)$$

where k = shape factor of approximate value 0.9, λ = wavelength of Cu*K*α radiation (λ = 1.5406 Å), β = FWHM and θ = diffraction angle (º).

The dislocation density (δ) of the electrode material was calculated by using the following formula [29]:

$$\delta = \frac{1}{D^2} \quad (2)$$

Microstrain (ε) was calculated by using eqn. 3 [30]:

$$\varepsilon = \frac{\beta \cos\theta}{4} \quad (3)$$

Table-1 displays the calculated parameters from the XRD data of crystal size, dislocation density and microstrain. The crystallite sizes were 16.19 nm, 15.45 nm, 13.23 nm and 15.14 nm, respectively. Therefore, the PEG-assisted CuO nanoparticles demonstrated a reduced crystallite size and was selected for further analysis.

FTIR studies: The functional groups of the surfactants assisted CuO nanoparticles were analyzed by FTIR spectra. As shown in Fig. 2, the assigned two characteristic peaks at 493 cm^{-1} and 610 cm^{-1} are attributed to ν(Cu-O) [31-33]. The presence of the broad peaks around at 3427 cm^{-1} is owing to

TABLE-1
STRUCTURAL PARAMETERS OF CuO NANOPARTICLES SYNTHESIZED WITH DIFFERENT SURFACTANTS

Sample	Crystallite size (nm)	Dislocation density, δ (lines/m^2)	Microstrain (ε) × 10^{-3}
Pure CuO	16.19	3.815	2.152
CTAB	15.45	4.189	2.247
PEG	13.23	5.715	2.622
HMTA	15.14	4.362	2.296

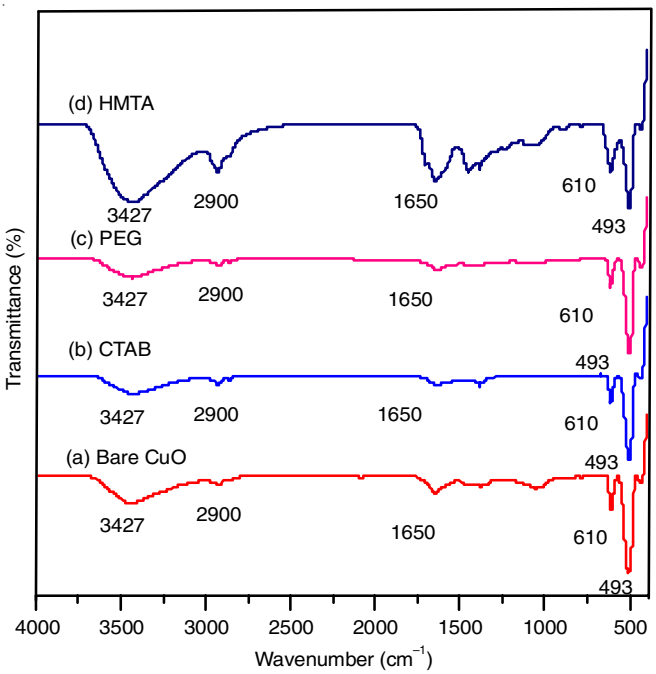

Fig. 2. FTIR spectra of CuO with different surfactants

stretching vibration of water molecule. The absorption band at 1650 cm^{-1} is usually ascribed to the bending modes of water molecules from atmosphere [34,35]. The weak absorption band position at 2900 cm^{-1} and all the samples are attributed to C-H bond as a stretching vibration [36].

SEM studies: The size of PEG-assisted CuO nanoparticles was significantly lower than that of other materials, indicating an improved specific surface area for electrochemical behaviour. Fig. 3a-h demonstrates that the structural variations are attributable to the influence of surfactants, in addition to the enhanced porosity of the PEG-assisted CuO nanoparticles [37,38]. The CuO NPs confirmed spherical like nanostructure in Fig. 3a-b, whereas the rock-like nanostructure was obtained by CTAB with CuO NPs as shown in Fig. 3c-d. In Fig. 3e-f, a rod like morphology is provided by PEG with CuO NPs, whereas Fig. 3g-h illustrates the twisted plate-like morphology of HMTA with CuO NPs. The several surfactants provided different particle size, which led to various microstructures with great potential candidate for supercapacitor applications [30-32]. The chemical composition of the synthesized CuO material was studied *via* EDX spectra, the Cu and O elements confirm presents in the prepared materials (Fig. 3i).

Fig. 4a-d revealed the histograms of particle size in the range of 30 nm, 29 nm, 15 nm and 23 nm for CuO NPs, CTAB CuO NPs, PEG-CuO NPs and HMTA-CuO NPs, respectively.

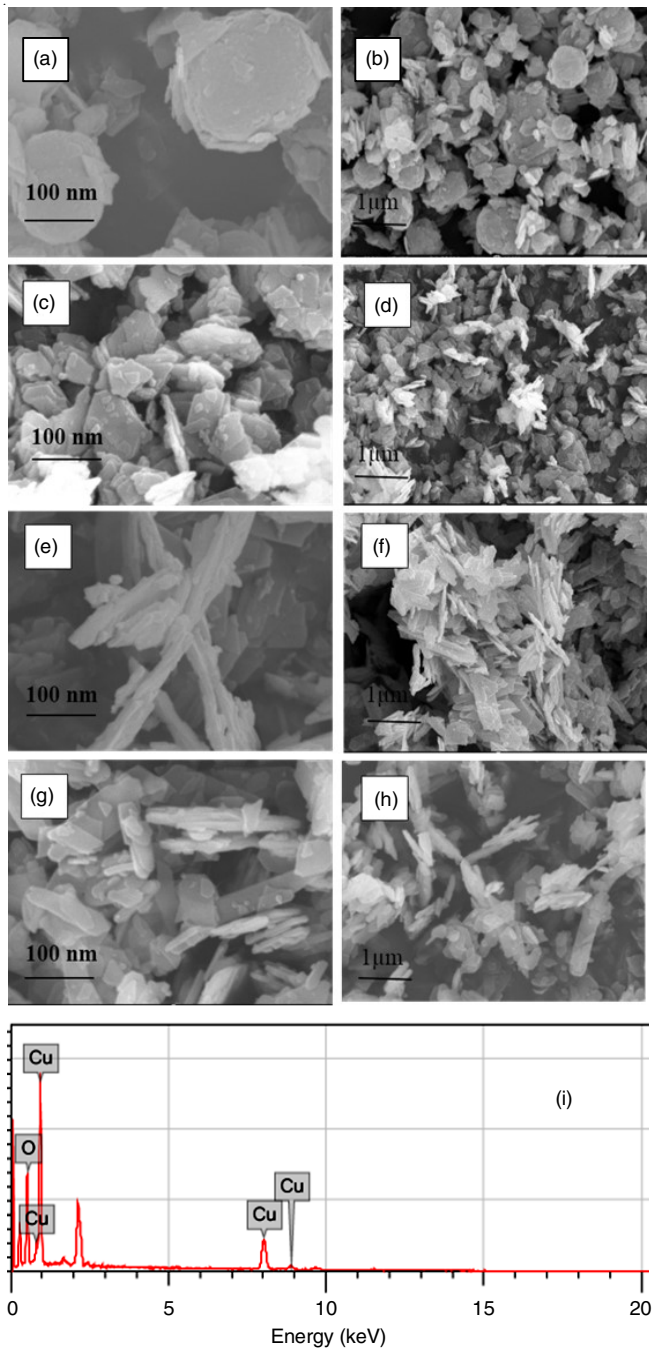

Fig. 3. SEM images of CuO_{bare} (a,b), CuO_{CTAB} (c,d), Cuo_{Peg} (e,f), CuO_{HMTA} (g,h) and EDX (i)

BET studies: The active surface area and pore size of the PEG-CuO nanoparticles were distributed by nitrogen adsorption and desorption isotherm curves. According to the IUPAC, the mesopore structure of the obtained nanomaterial is type IV, as shown in Fig. 5a-b. The calculated active surface area and pore size were found to be 11.38 m^2 g^{-1} and ~50 nm, respectively, which is suitable for the electrochemical applications [38]. Furthermore, the surface area of PEG-CuO NPs was increased owing to the enhancement of the pores, which yielded the high capacitance property.

XPS studies: XPS analysis is conducted to investigate the atomic states of PEG-CuO NPs. Fig. 6a shows the spectrum

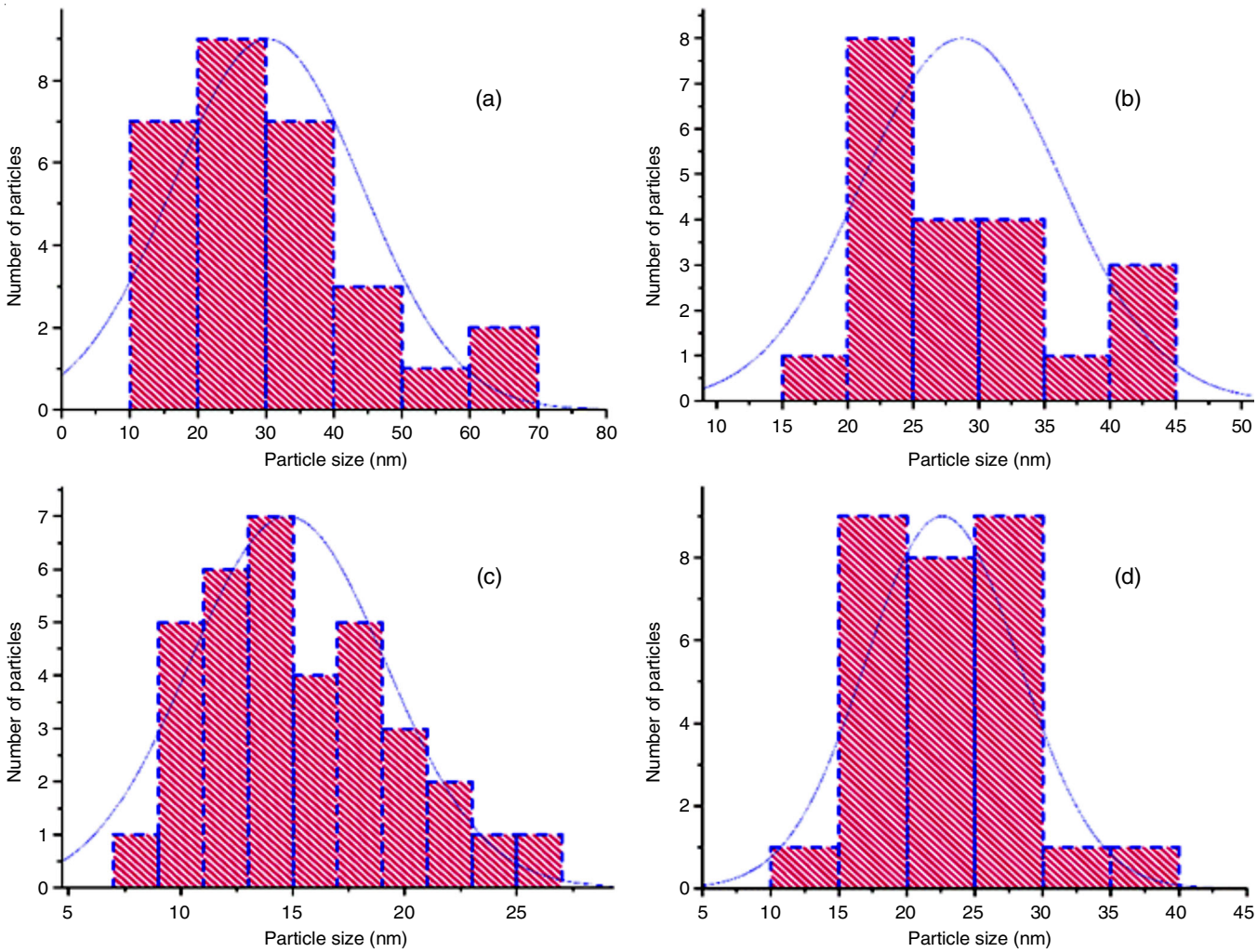

Fig. 4. Particle size distribution histograms in CuO nanoparticles, (a) bare, (b) CuO + CTAB, (c) CuO + PEG and (d) CuO + HMTA

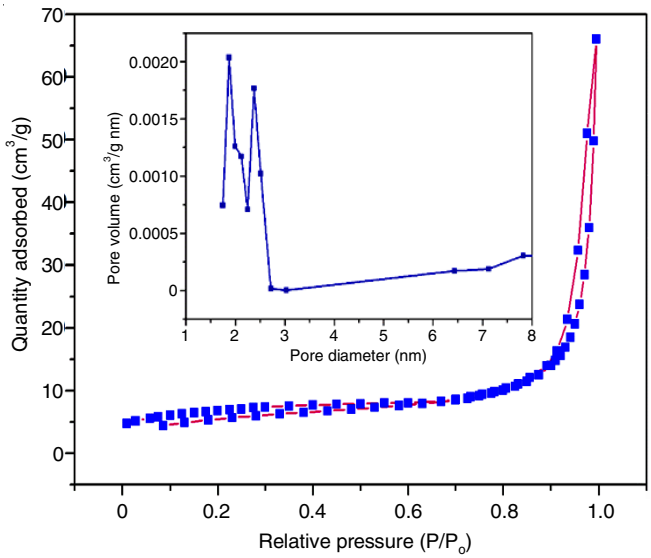

Fig. 5. Nitrogen adsorption and desorption isotherms and the corresponding pore size distribution curve (inset) of bare CuO nanoparticles

of the prepared copper oxide nanoparticles, confirms the presence of both elements (Cu and O). Fig. 6b-c illustrates the core level spectra of Cu 2p and O 1s in the prepared samples. Fig. 6b demonstrated the spectrum of Cu, the Cu 2p peaks found with doublet-fitted peaks at 934.46 eV (Cu $2p_{1/2}$) and 935.10 eV (Cu $2p_{3/2}$) [39,40]. Furthermore, the O 1s in the XPS spectrum (Fig. 6c) exposed two peaks are revealed at 530.53 eV and 531.32 eV [41,42].

Electrochemical properties

Cyclic voltammetry (CV): The CV measurements for CuO NPs was performed using a three electrode cell combinations system 1 M Na_2SO_4 electrolyte. Fig. 7a illustrates the CV curves of the synthesized product at various scan rates from 10-100 mV s^{-1} in potential windows of 0.05-0.50 V. The main characteristics of ideal materials are the rectangular shape, which exhibits the pseudocapacitive behaviour of the synthesized product [43].

The capacitance values of the prepared electrode material were calculated from the CV curves from the following relation [44]:

$$C_s = \frac{s}{mk\Delta V} \quad (4)$$

where s = the specific area of CV curve; m = mass of active electrode; k = scan rate (mV/s) and ΔV = the potential window.

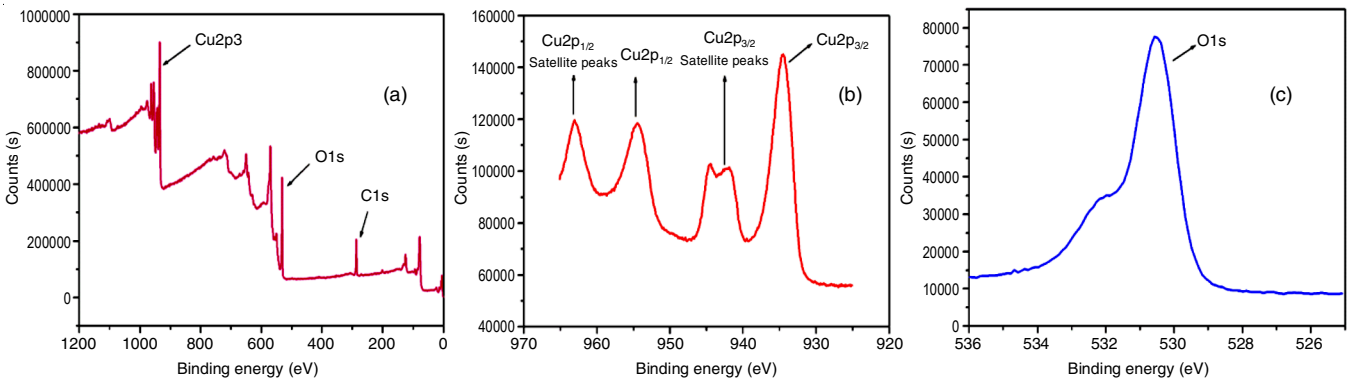

Fig. 6. (a) XPS survey spectra of CuO nanoparticles and (b) core level spectra of Cu 2p, (c) O1s

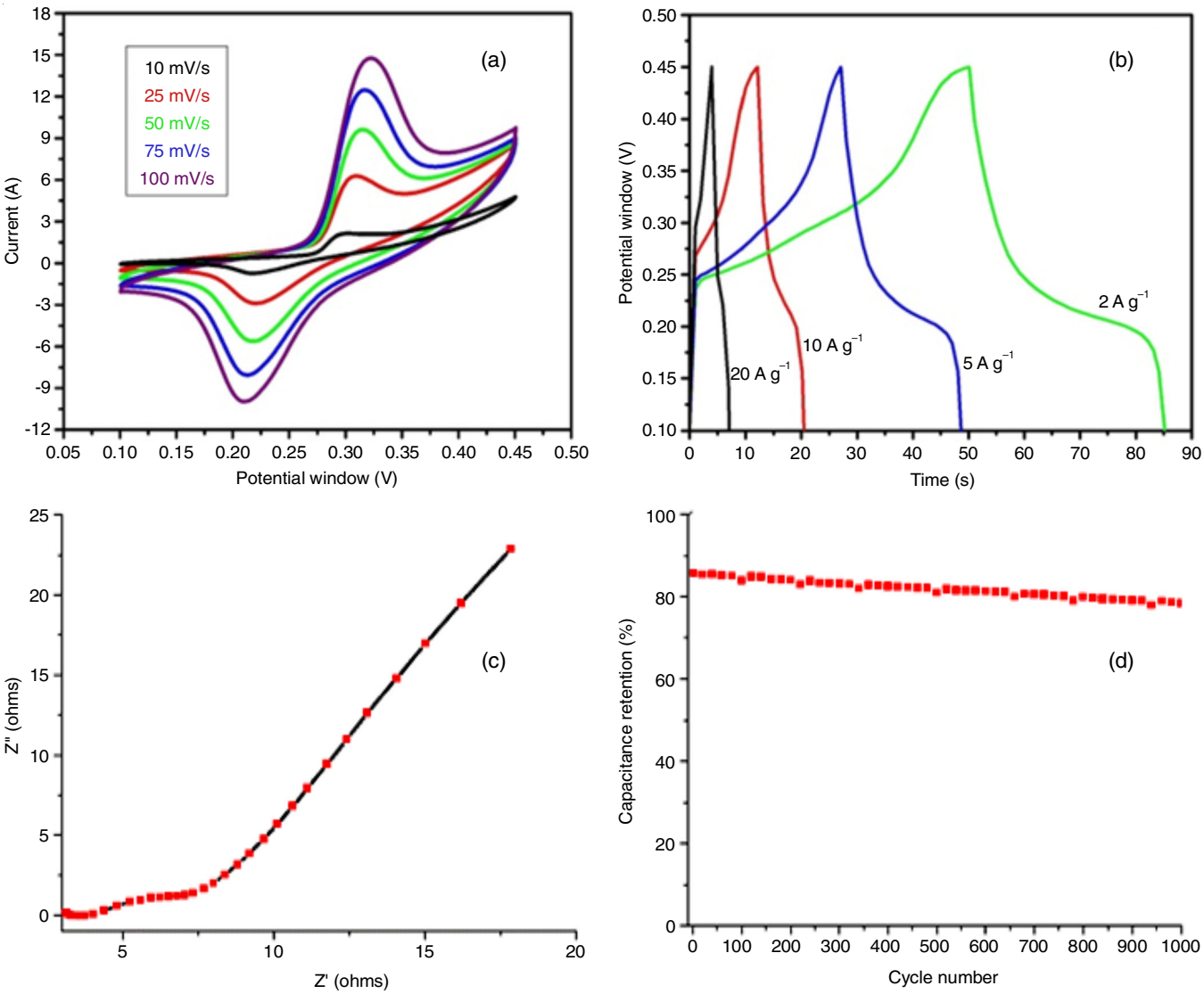

Fig. 7. (a) Plot of cyclic voltagram of CuO nanoparticles at various scan rates, (b) galvanostatic charge/discharge curve, (c) Nquist plot of CuO nanoparticles electrode, (d) cycle stability and capacitance retention of CuO electrode

The calculated C_{sp} values of the CuO electrode (eqn. 4) were found to be 297, 275, 251, 186 and 153 F g^{-1} at diverse scan rate of 10, 25, 50, 75 and 100 mV/s. However, the obtained specific capacitance values continuously reduced in the CV loop with increasing scan rates. The electrode interacts with the working electrode rapidly due to the limited mobility of ions, which cannot reach the inner active site within the sufficient time [45]. These results proved that the CuO electrode (rod like) nanostructure is more suitable for supercapacitor applications [46].

Galvanostatic charge-discharge (GCD) studies: Fig. 7b illustrates the GCD curves recorded in a 1 M Na_2SO_4 solution at varying current densities of 1, 2, 3 and 4 A/g. The charging/discharging curves were almost symmetrical triangular shapes and also exhibit a good linear variation, which proved excellent electrochemical performance [47].

From the GCD curves, the C_{sp} values of the prepared nanomaterials can be calculated using eqn. 5 [48]:

$$C_{sp} = \frac{I \times \Delta t}{m \times \Delta v} \quad (5)$$

The applied current (mA), the discharge time of GCD curves (s), the applied potential windows (V) and the mass of the active material (mg) are I, Δt, Δv and m, respectively.

The C_{sp} values are found to be 153, 147, 110, and 87 F/g at the current densities of 1, 2, 3, and 4 A/g, respectively. The obtained capacitance value decreased with increased current density. The outstanding cyclic stability of the PEG-CuO NPs can be mainly determined by its rod-like structure and low crystallite size, which provide a suitable active surface area for ion transition. These results showed that the PEG-CuO active electrode (mesoporous structure) is a promising candidate for the supercapacitor applications [49].

Electrochemical impedance spectroscopy (EIS): As shown in Fig. 7c, the electrical conductivity and ion transfer of the prepared electrode was investigated by EIS [45,46]. The Nyquist plots demonstrate the superior electrochemical behavior of PEG-CuO electrodes. In the high-frequency region, the semicircle exhibited a depression, indicating of electrolyte resistance attributed to the faradic reaction. A vertical linear spike is predicted along the imaginary axis in low frequency areas that results indicate pseudocapacitance characteristic features of the product [50]. The prepared PEG-CuO nanomaterial has outstanding performance for electrochemical applications.

Cycle stability: To assess the cycle stability of the prepared PEG-CuO electrode material and investigate its potential applications, GCD profiles were conducted over 1,000 cycles at a current density of 0.25 A g^{-1}. According to Fig. 7d, the CuO NPs electrode exhibits exceptional cycling performance, with almost 77.24% capacitance retention up to 1,000 cycles [49]. The result indicated that the reduced particle size, accessible surface area and shorter ion/electron transfer channels of PEG-CuO NPs rod-like structure could be suitable candidates for electrochemical applications. Additionally, the synthesized nanoparticles demonstrated improved mechanical power and long-term charge-discharge with exceptional cycling capability.

Conclusion

The CuO nanostructures were successfully prepared with different surfactants (CTAB, PEG and HMTA) *via* a simple hydrothermal route. The XRD profile revealed the orthorhombic structure of surfactant-mediated CuO nanoparticles. The different surface morphologies, such as spherical, rock-like rod-like and plate-like were observed through SEM images. The BET results distributed an enhance in the active surface area of the prepared nanostructures. The PEG-assisted CuO shows a very high capacitance of 297 F g^{-1} at 10 mV s^{-1}. Hence, this nanostructure enhanced the electrochemical behaviour of prepared electrodes at low scan rates. The PEG-assisted CuO NPs have retention of 77.24% after 1,000 cycles, which is suitable for the electrochemical applications.

CONFLICT OF INTEREST

The authors declare that there is no conflict of interests regarding the publication of this article.

REFERENCES

1. Y. Lu, Z.A. Khan, M.S. Alvarez-Alvarado, Y. Zhang, Z. Huang and M. Imran, *Sustainability*, **12**, 5078 (2020); https://doi.org/10.3390/su12125078
2. M. Vijayakumar, A. Bharathi Sankar, D. Sri Rohita, T.N. Rao and M. Karthik, *ACS Sustain. Chem.& Eng.*, **7**, 17175 (2019); https://doi.org/10.1021/acssuschemeng.9b03568
3. A.K. Yedluri and H.-J. Kim, *RSC Adv.*, **9**, 1115 (2019); https://doi.org/10.1039/C8RA09081E
4. C. Yan, M. Jin, X. Pan, L. Ma and X. Ma, *RSC Adv.*, **10**, 9299 (2020); https://doi.org/10.1039/C9RA10701K
5. M. Minakshi S. Higley, C. Baur, D.R.G. Mitchell, R.T. Jones and M. Fichtner, *RSC Adv.*, **9**, 26981 (2019); https://doi.org/10.1039/C9RA04289J
6. L. Chen, D. Liu and P. Yang, *RSC Adv.*, **9**, 12793 (2019); https://doi.org/10.1039/C9RA01928F
7. B.A. Mola, G. Mani, S. Sambasivam, M.R. Pallavolu, A.A. Ghfar, M. Ouladsmane, M. Alsawat, N.R. Reddy, Y. Noh, S.K. Jilcha, H.J. Kim, I.M. Obaidat and Y.A. Kumar, *J. Energy Storage*, **43**, 103155 (2021); https://doi.org/10.1016/j.est.2021.103155
8. P. Simon and Y. Gogotsi, *Acc. Chem. Res.*, **46**, 1094 (2013); https://doi.org/10.1021/ar200306b
9. J. Liu, J. Wang, C. Xu, H. Jiang, C. Li, L. Zhang, J. Lin and Z.X. Shen, *Adv. Sci.*, **5**, 1700322 (2018); https://doi.org/10.1002/advs.201700322
10. F. Chen, C. Chen, Q. Hu, B. Xiang, T. Song, X. Zou, W. Li, B. Xiong and M. Deng, *Chem. Eng. J.*, **401**, 126145 (2020); https://doi.org/10.1016/j.cej.2020.126145
11. K. Kierzek and G. Gryglewicz, *Molecules*, **25**, 4255 (2020); https://doi.org/10.3390/molecules25184255
12. R. He, G. Xu, Y. Wu, K. Shi, H. Tang, P. Ma, J. Zeng, Y. Bai and S. Chen, *Int. J. Hydrogen Energy*, **44**, 5940 (2019); https://doi.org/10.1016/j.ijhydene.2019.01.114
13. D.S. Gavaskar, P. Nagaraju, Y. Vijayakumar, P.S. Reddy and M.V.R. Reddy, *J. Asian Ceram. Soc.*, **8**, 605 (2020); https://doi.org/10.1080/21870764.2020.1769820
14. D.D. Vuong, L.H. Phuoc, V.X. Hien and N.D. Chien, *Mater. Sci. Semicond. Process.*, **107**, 104861 (2020); https://doi.org/10.1016/j.mssp.2019.104861
15. S.D. Dhas, P.S. Maldar, M.D. Patil, A.B. Nagare, M.R. Waikar, R.G. Sonkawade and A.V. Moholkar, *Vacuum*, **181**, 109646 (2020); https://doi.org/10.1016/j.vacuum.2020.109646
16. L. Kunhikrishnan and R. Shanmugam, *J. Mater. Sci. Mater. Electron.*, **31**, 21528 (2020); https://doi.org/10.1007/s10854-020-04665-0
17. J. Toupin, H. Strubb, S. Kressman, V. Artero, N. Krins and Ch Laberty-Robert, *J. Sol-Gel. Sci. Technol.*, **89** 255 (2019); https://doi.org/10.1007/s10971-018-4896-3
18. H. Siddiqui, M.R. Parra, P. Pandey, M.S. Qureshi and F.Z. Haque, *J. Sci.-Adv. Mater. Device*, **5**, 104 (2020); https://doi.org/10.1016/j.jsamd.2020.01.004
19. B. Guo, M. Košiček, J. Fu, Y. Qu, G. Lin, O. Baranov, J. Zavašnik, Q. Cheng, K. Ostrikov and U. Cvelbar, *Nanomaterials*, **9**, 1405 (2019); https://doi.org/10.3390/nano9101405
20. X. Wei, X. Wang, B. Gao, W. Zou and L. Dong, *ACS Omega*, **5**, 5748 (2020); https://doi.org/10.1021/acsomega.9b03787

21. J. Lu, W. Xu, S. Li, W. Liu, M.S. Javed, G. Liu and C. Hu, *J. Mater. Sci.*, **53**, 739 (2018); https://doi.org/10.1007/s10853-017-1493-8
22. M.S. Alqahtani, N.M.A. Hadia and S.H. Mohamed, *Optik*, **173**, 101 (2018); https://doi.org/10.1016/j.ijleo.2018.08.016
23. A. Albert manoharan, R. Chandramohan, R. David prabu, S. Valanarasu, V. Ganesh, M. Shkir, A. Kathalingam and S. AlFaify, *J. Mol. Struct.*, **1171**, 388 (2018); https://doi.org/10.1016/j.molstruc.2018.06.018
24. G. Akarken, U. Cengiz and T.E. Bektas, *J. Adv. Res. Nat. Appl. Sci.*, **10**, 329 (2024); https://doi.org/10.28979/jarnas.1405595
25. Z.R. Parekh, S.H. Chaki, A.B. Hirpara, G.H. Patel, R.M. Kannaujiya, A.J. Khimani and M.P. Deshpande, *Physica B*, **610**, 412950 (2021); https://doi.org/10.1016/j.physb.2021.412950
26. D. Ghosh, S. Bhandari and D. Khastgir, *Phys. Chem. Chem. Phys.*, **18**, 32876 (2016); https://doi.org/10.1039/C6CP06611A
27. S.M. Keshk, A.M. Ramadan and S. Bondock, *Carbohydr. Polym.*, **127**, 246 (2015); https://doi.org/10.1016/j.carbpol.2015.03.038
28. J.S.K. Arockiasamy and C. Johnson, *Cermaic Int.*, **42**, 6198 (2016); https://doi.org/10.1016/j.ceramint.2015.12.180
29. M. Figiela, M. Wysokowski, M. Galinski, T. Jesionowski and I. Stepniak, *Sens. Actuators B Chem.*, **272**, 296 (2018); https://doi.org/10.1016/j.snb.2018.05.173
30. S. Suthakaran, S. Dhanapandian, N. Krishnakumar and N. Ponpandian, *J. Mater. Sci. Mater. Electron.*, **30**, 13174 (2019); https://doi.org/10.1007/s10854-019-01681-7
31. K.K. Sahu, B. Raj, S. Basu and M. Mohapatra, *ACS Omega*, **6**, 1108 (2021); https://doi.org/10.1021/acsomega.0c03899
32. P.E. Lokhande and U.S. Chavan, *Inorg. Nano-Met. Chem.*, **48**, 434 (2018); https://doi.org/10.1080/24701556.2019.1569685
33. B. Saravanakumar, C. Radhakrishnan, M. Ramasamy, R. Kaliaperumal, A.J. Britten and M. Mkandawire, *Results Phys.*, **13**, 102185 (2019); https://doi.org/10.1016/j.rinp.2019.102185
34. A.M. Teli, G.J. Navathe, D.S. Patil, P.R. Jadhav, S.B. Patil, T.D. Dongale, M.M. Karanjkar, J.C. Shin and P.S. Patil, *Sustain. Energy Fuels*, **1**, 377 (2017); https://doi.org/10.1039/C6SE00016A
35. M. He, L. Xie, X. Zhao, X. Hu, S. Li and Z.-G. Zhu, *J. Alloys Compd.*, **788**, 36 (2019); https://doi.org/10.1016/j.jallcom.2019.01.349
36. D. Meng, D. Liu, G. Wang, X. San, Y. Shen, Q. Jin and F. Meng, *Vacuum*, **144**, 272 (2017); https://doi.org/10.1016/j.vacuum.2017.08.013
37. V.A. Shmatko, A.A. Ulyankina, N.V. Smirnova and G.E. Yalovega, *Opt. Spectrosc.*, **124**, 478 (2018); https://doi.org/10.1134/S0030400X18040161
38. M. Rawat and D.S. Rawat, *ACS Sustain. Chem.& Eng.*, **8**, 13701 (2020); https://doi.org/10.1021/acssuschemeng.0c03898
39. S.K. Shinde, S.M. Mohite, A.A. Kadam, H.M. Yadav, G.S. Ghodake, K.Y. Rajpure, D.S. Lee and D.-Y. Kim, *J. Electroanal. Chem.*, **850**, 113433 (2019); https://doi.org/10.1016/j.jelechem.2019.113433
40. N. Mohammadi, K. Pourreza, N. Bahrami Adeh and M. Omidvar, *J. Alloys Compd.*, **883**, 160874 (2021); https://doi.org/10.1016/j.jallcom.2021.160874
41. M. Xu, N. Fu, X. Wang and Z. Yang, *J. Mater. Sci. Mater. Electron.*, **31**, 16027 (2020); https://doi.org/10.1007/s10854-020-04165-1
42. S.K. Shinde, H.M. Yadav, G.S. Ghodake, A.A. Kadam, V.S. Kumbhar, J. Yang, K. Hwang, A.D. Jagadale, S. Kumar and D.Y. Kim, *Colloids Surf. B Biointerfaces*, **181**, 1004 (2019); https://doi.org/10.1016/j.colsurfb.2019.05.079
43. K. Ashokkumar, S. Dhanapandian, S. Suthakaran and N. Krishnakumar, *Mater. Technol.*, **37**, 2861 (2022); https://doi.org/10.1080/10667857.2022.2083483
44. D. Govindarajan, F.J. Johanson, V. Uma shankar, M.J. Salethraj and R. Gopalakrishnan, *J. Mater. Sci. Mater. Electron.*, **32**, 19434 (2021); https://doi.org/10.1007/s10854-021-06460-x
45. A. Ray, A. Roy, M. Ghosh, J.A. Ramos-Ramón, S. Saha, U. Pal, S.K. Bhattacharya and S. Das, *Appl. Surf. Sci.*, **463**, 513 (2019); https://doi.org/10.1016/j.apsusc.2018.08.259
46. K.M. Racik, A. Manikandan, M. Mahendiran, P. Prabakaran, J. Madhavan and M.V.A. Raj, *Physica E*, **119**, 114033 (2020); https://doi.org/10.1016/j.physe.2020.114033
47. A. Ghosh, M. Miah, A. Bera, S.K. Saha and B. Ghosh, *J. Alloys Compd.*, **862**, 158549 (2021); https://doi.org/10.1016/j.jallcom.2020.158549
48. H. Shi, M. Ma, P. Liu, X. Jia, F. Yang, B. Zhao and Z. Li, *J. Electroanal. Chem.*, **876**, 114481 (2020); https://doi.org/10.1016/j.jelechem.2020.114481
49. B. Padmaja, S. Dhanapandian and K. Ashokkumar, *Mater. Sci. Eng. B*, **297**, 116699 (2023); https://doi.org/10.1016/j.mseb.2023.116699
50. Y. Zhan, J. Bai, F. Guo, H. Zhou, R. Shu, Y. Yu and L. Qian, *J. Alloys Compd.*, **885**, 161014 (2021); https://doi.org/10.1016/j.jallcom.2021.161014